Improved the in-Situ Remediation Effect of Sediment Microbial Fuel Cells by Optimizing the Anode Structure

Henan Li
North China Municipal Engineering Design and Research Institute https://orcid.org/0000-0003-3338-1981

Guohong Liu
Harbin Institute of Technology School of Environment

Chao Li
Daqing Oilfield Co Ltd

Yongli Sun
North China Municipal Engineering Design and Research Institute

Yujie Feng (yujief@hit.edu.cn)
Harbin Institute of Technology School of Environment https://orcid.org/0000-0002-0686-3937

Research Article

Keywords: Sediment, In-situ remediation, Bio-electrochemical Systems, Anode

Posted Date: November 2nd, 2021

DOI: https://doi.org/10.21203/rs.3.rs-1014336/v1

Abstract

Six 60-L benthic microbial electrochemical systems (BMES) were built for the bioremediation of river sediment. Carbon mesh anodes with honeycomb-structure supports were compared with horizontal anodes, and the system was tested using different cover depths and anode densities. The pollutant removal, electricity generation, and electrochemistry of the six BMES with different anodes was examined using the Ashi River (Harbin, China) as a case study. Total organic carbon (TOC) and total nitrogen (TN) removal from sediments in BMES with three-dimensional anodes were 20%~30% and 20%~33% higher for the other reactors. Moreover, the honeycomb-structure of the anode also resulted in higher power density and improved humus removal.

1 Introduction

Sediments accommodate various inorganic and organic water pollutants arising from human activities, including nutrient elements and refractory complex organic pollutant, as the most important repositories of the overlying water body. (Beg et al. 2001). The sediments also shelter a complex microbial ecosystem that thrives on several different electron donors and acceptors, and functions in the degradation of the accumulated pollutions(Martins et al. 2014a; Martins et al. 2014b; Bolam et al. 2006). Usually, the accumulation reductive substance and a lack of accessible electron acceptors are the main limitations for the remediation of underwater sediments in anaerobic conditions(De Schamphelaire et al. 2008; Song et al. 2011). Bio-electrochemical Systems (BESs) utilize anode-respiring microorganisms as catalysts, they can generate electricity from the oxidation of organic or inorganic matter and does not need in situ addition of electron donor or electron acceptor into the subsurface(Zhang et al. 2015; Lovley 2006). The Benthic Microbial Electrochemical Systems (BMESs), with its anode embedded in the sediment and its cathode suspended in aerobic water, could be utilized for sediment bioremediation(Zhu et al. 2015).

Recently, numerous studies have applied BMES to the bioremediation of sediments in freshwater environments(Kouzuma et al. 2014; Yang et al. 2015; Li and Yu 2015). BMES has been performed with a volume of 0.25 L for the treatment of phenol-contaminated soil in the anode chamber and 90% of phenol was removed from the polluted soil, while only 13% was removed from an open-circuit control(Deng et al. 2014). A 22 L BMES with graphite plate electrodes has demonstrated effective cellulose degradation from aquaculture pond sediment(Sajana et al. 2014). Researchers have reported that the electrical power of BMES is controlled by the organic content of the sediment; the greater of organic content, the higher the current and power density (PD) that can potentially be produced(Virdis et al. 2008; Villasenor et al. 2013; Beg et al. 2001). However, studies of large-scale BMES for in situ remediation of natural sediments remain limited.

The anode material, geometry, and surface modifications are the key parameters in optimizing electricity harvesting from sediments. These parameters affect microbial adhesion to the anode surface, electron transfer, and substrate oxidation; moreover, they affect the performance of the SMFC (Zabihallahpoor et al. 2015; Zhang et al. 2015; Teleken et al. 2017). Various types of materials have been used as electrodes.

Nevertheless, there is still room to improve electrode materials and to optimize the performance of SMFCs. In a comparison of SMFC reactors with carbon fiber cloth and carbon felt as anodes, the carbon fiber cloth model showed the best performance (33.5±1.5 mW/m^2)(Song et al. 2012). Air-cathode SMFCs with anodes horizontally and vertically arranged yielded charge outputs of up to 833 and 762 C, respectively. Considering both the enhanced biodegradation of hydrocarbons and generation of charge, SMFCs with horizontally arranged anodes are a promising tool for future applications(Zhang et al. 2015). The possibility of maintaining high power density at scaled-up BMFCs was explored by arranging multiple anodes in sediment. Multiple anodes with multiple collectors effectively utilized sediment in both the horizontal and vertical directions, and enhanced electron collection efficiency(Bingchuan Liu. 2016). The anode potential of SMFCs is an important parameter for determining the anode depth to optimize power generation. Five rigid graphite plates were embedded in evenly divided sections of sediment to compare the performances of SMFCs having anode electrodes horizontally embedded at different depths. The maximum power and current of the SMFCs increased in depth order, the anode-embedding depth is also an important parameter to determine the performance of SMFCs(An et al. 2013).

The main purpose of this study was to compare the remediation of sediments in when using different configurations of anodes. Six 60-L BMES were built for the bioremediation of river sediment, using the Ashi River (Harbin, China) as a case study. Carbon mesh anodes with honeycomb-structure supports were compared with horizontal anodes at different cover depths and anode densities. Organic pollutant removal from both water and sediment was investigated. Finally, the electricity generation and electrochemistry of the six BMES were sustainability studied.

2 Materials And Methods

2.1 Reactor construction and electrodes

Plexiglas plate with a thickness of 10 mm were used to manufacture BMESs. The total empty bed volume of BMES was 75 L, 60 cm in length, 25 cm in width, and 65 cm in height for the inner dimensions. Sediment(taken from the Ashi River, Harbin, China) was laid 15 cm thick on the bottom of the reactor. The water layer was 30 cm deep over the sediment layer with a total volume of 45 L. In total, the volume of the BMES was 67.5 L with water and sediment.

Carbon mesh anodes with honeycomb-structure supports was constructed through heat-presse(Fig.S1). The external resistance between the honeycomb-structure anode and air cathode was set at 500 Ω. The honeycomb-structure anode (L × W × H: 45 × 25 × 10 cm) was buried in the bottom of the river sediment; air cathodes (L × W: 20 × 10 cm) with activated carbon catalyst layers(Dong et al. 2012) were placed above the water. The distance between the anode and the cathode was 35 cm.

To investigate the influence of anode area, the areas (anode) of carbon cloths were 400, 600, or 1200 cm^2 (BMES1, BMES2, and BMES3, respectively), covering 50%, 30%, and 100% of the bottom area of the reactor, respectively. Horizontal anodes with the same area as the bottom area were used in BMES3 and

BMES4; they were buried by 15 and 7.5 cm thick sediments, respectively, to investigate the effect of anode depth. We used honeycomb-structure anodes to obtain the same surface area as used in BMES5 and BMES6; these were buried by 15 and 7.5 cm thick sediments, respectively, to investigate the effect of anode depth(Fig. 1).

2.2 Operation of BMES

The BMES was operated in batch mode, the solution in the reactor was recycled by a submerged pump at a reflux rate of 400 L h^{-1}, simulating the hydraulic scouring of river water.

Table 1 Reactor settings

	BMES 1	BMES 2	BMES 3	BMES 4	BMES 5	BMES 6
L/W/H (cm)	50/24/50	50/24/50	50/24/50	50/24/50	50/24/50	50/24/50
Cathode area（cm^2）	400	600	1200	1200	1200	1200
Anode structure	horizontal anode	horizontal anode	horizontal anode	horizontal anode	honeycomb-structure Anode	honeycomb-structure Anode
Anode depth（cm）	15	15	15	7.5	15	7.5

Two sediment-sampling points within the anode zone were set on the centerline 20 and 40 cm from the bottom plate along the flow path. The sediment samples taken from these two sampling points were analyzed as duplicates. At each sampling point, the sediment samples around the anode were taken out of the reactor from the top using a gravity core sampler. All the sediment samples were sieved through a 0.5-cm sieve to remove coarse debris and mechanically homogenize the material. Then, the sediment samples were temporarily stored in refrigerator at -40°C prior to analysis and experiments. Water samples were taken for water quality analysis.

Water quality analyses were conducted by testing the concentrations of TOC (total organic carbon), TN (total nitrogen), and NH+ 4-N (ammonium) in the effluent using standard methods(E.W. Rice et al. 2017). Excitation-emission matrices (EEMs) were investigated at the end of the operation. Fluorescence EEM measurements were conducted using a Perkin-Elmer LS-50B luminescence spectrometer. The sediment samples weretaken for the TOC and TN measurements(E.W. Rice et al. 2017).

2.3 Analysis and calculation methods

Voltage data between the anode and cathode was recorded by data acquisition system (PISO-813.ICP DAS CO, Ltd). The power output was calculated according to P = UI. Ag/AgCl electrodes were located beside the floating cathode in the water layer over the sediment. Power density (mW m^{-2}) and current density (mA m^{-2}) were normalized over the cathodic area (0.02 m^2). Electrochemical impedance

spectroscopy (EIS) was performed at a cathode potential of 0.1 V over a frequency range of 100 kHz to 10 mHz with an amplitude of 10 mV. The experimental data were interpreted with an equivalent circuit Rohm [Q(RctW)] using the Zsimpwin software 3.10(Hutchinson et al. 2011). In this equivalent circuit, the Rohm component represents for ohmic resistance, Rct, for charge transfer resistance.

3 Results And Discussion

3.1 Electricity generation

The average voltage outputs were 232, 397, 383, 373, 455, and 321 mV for BMES1, BMES5, BMES2, BMES3, BMES4, BMES5, and BMES6, respectively. Voltage output for BMES5 was the highest, while that of BMES1 was the lowest. During operation, voltage outputs of BMES1, BMES2, and BMES3 descended in the order of BMES2 > BMES3 > BMES1, showing that lower anode area (33% of the floorage) decreased the low voltage. The voltage of BMES2 was close to that of BMES3; that is, increasing the anode area from 30–50% was conducive to improving the voltage output. However, increasing the anode area from 50–100% had little impact on the voltage output. Therefore, changes of anode area within a certain range do not affect the voltage output of the reactor.

The influence of different anode structures on the voltage output of the BMES systems was compared. The anode embedded depths in BMES3 and BMES5 were both 15 cm. The voltage output of BMES5 was 455 mV, 18.8% higher than that of BMES3 (383 mV), showing that honeycomb-structure anodes are more favorable for producing higher voltage output than are horizontal anode reactors. The voltage output of BMES4 was 16.2% higher than that of BMES6, confirming that honeycomb-structure anodes exhibit higher voltage output.

The voltage outputs of the anodes at different depths were also compared(Fig. 2). When the anode was buried at 15 cm depth, the voltage output was 5%□26% higher than when the anode was buried at 7.5 cm depth. That is, honeycomb-structure anode performance is significantly affected by burial depth. This indicates that the thickness of sediment cover above an anode can affect the voltage output of the whole reactor. Electrochemically active bacteria usually live in an anaerobic or anoxic environment(Holmes et al. 2004; Leang et al. 2005), which is the main reason why the anode of a BMES system usually operates under anaerobic conditions. Oxygen or other substances or factors that lead to the increase of redox potential will directly affect the working efficiency of the anode and the inactivation of electrochemical active bacteria and related microorganisms in the anode region, leading to system collapse(Oon et al. 2016; Lovley 2006). We found that the burial depth of the anode in sediments will directly affect the power output of the BMES system; to ensure the performance of the system, the burial depth of the anode should be no less than 15 cm.

Polarization tests were performed to reveal the power generation performance of the BMES. The maximum power densities were 29.3, 40.0, 37.1, 39.2, 49.7, and 43.2 mW m^{-2} for BMES1, BMES5, BMES2, BMES3, BMES4, BMES5, and BMES6, respectively. The maximum power densities in BMES with

honeycomb-structure anodes (BMES5 and BMES6) were 10%–40% higher than for BMESs with horizontal anode reactors (BMES3 and BMES4). The maximum power density in BMES5 (honeycomb-structure anode buried at 15 cm depth) was 15% higher than that in BMES6 (honeycomb-structure anode buried at 7.5 cm depth). The maximum power densities of BMES2 and BMES3 indicated increasing the anode area is conducive to improving the power output of BMES systems.

EIS data for each anodes were obtained to further analyze the law and mechanism of the influence of different anode structures on the electronic transfer of the system. A Nyquist plot was used to show the fitting results. In general, BMES internal resistance (Rin) can be divided into three types: ohm internal resistance (Rohm), charge transfer internal resistance (Rct), and diffusion internal resistance (Rd) (Karthikeyan et al. 2015; Hutchinson et al. 2011). Among them, the ohmic resistance is mainly caused by the battery configuration, electrode material resistance, and solution resistance. The diffusion resistance is due to mass transfer loss caused by material migration to the electrode surface. The internal resistance of charge transfer is mainly caused by electrode reaction, which includes redox reactions and activation loss during electron transfer(Karthikeyan et al. 2015; Feng et al. 2014). Microorganisms act as catalysts on the anode. Their growth and domestication are closely related to substrate metabolism and electron transfer, and the resistance caused by them is mainly the internal resistance of charge transfer. In this study, the ohm internal resistance of each reactor was between ~34.1 and 53 Ω; BMES2 and BMES3 had the greatest ohm internal resistance, indicating that anode areas of less than 30% and/or anode burial depths of less than 7.5 cm are not conducive to reducing ohmic internal resistance. The internal mass transfer resistances of BMES1 and BMES2 (4.7–97 Ω) were much higher than those of other reactors, indicating small anode area (30%~50% of the bottom area of the reactor) is not conducive to reducing internal mass transfer resistance. The mass transfer resistances of BMES5 and BMES6 were 5.7 and 4.7 Ω, respectively(Fig. 3), only 30% and 19.3% of the internal mass transfer resistance in BMES3 and BMES4. This shows that a honeycomb-structure anode structure reduces the reactor mass transfer resistance. The electrochemical performance analysis results show that differences in reactor performance were mainly due to the high and low anode performances. The electrochemical performances of honeycomb-structure anode structures are better than those of planar anode structures; moreover, larger area anodes and greater burial depths (15 cm) are optimal.

3.2 Water treatment

TOC and TN content change in water

Over 60 days off operation, the average TOC concentrations were 10.58, 9.13, 9.30, 9.70, 8.39, and 9.88 mg/L in BMES1–BMES6(Fig. 4a). The TOC concentration in BMES1 was 14%–16% higher than those in BMES2 and BMES3, while the TOC concentration in BMES2 was close to that in BMES3. As such, we infer that some reduction in the anode area does not influence TOC removal in BMES, but that pollutant removal may decline if the anode area reaches just 30% of the bottom area of the reactor.

The average TN concentrations were 19.42, 20.47, 21.24, 20.15, 20.62, and 25.34 mg/L in BMES1–BMES6(Fig. 4b). Except for some abnormal data points, the TN content in the upper water body

remained below 30 mg/L during the operation of all reactors. The TN content in BMES6 was higher than that of other the reactors owing to numerical anomalies of individual data points; the average values of TN in the other reactors were relatively close.

EC, DO, and pH change in water

The average values of EC, DO, and pH were measured daily. Increasing the anode area (from 30–50%) was conducive to reducing the EC content in the water body. However, when the anode area increased from 50–100%, the EC content in the upper water body was not significantly affected. When the anode was buried at 15 cm depth, the anode with the honeycomb-structure structure facilitated reduced EC in the water body compared with planar anodes. However, when the burial depth of the anode was 7.5 cm, the EC content of the reactor with a honeycomb-structure structure was 11.6% higher than that for the planar anode. As such, EC content of the upper water body can be better controlled when the burial depth of the anode reaches a certain degree (15 cm), and the water quality can be improved by controlling the anode depth.

The concentrations of dissolved oxygen in BMES1, BMES2, and BMES5 (5.05~5.75 mg/L) were slightly higher than those in BMES3, BMES4, and BMES6 (4.12~4.69 mg/L).

TOC, EC, and DO contents in BMES1 were higher than those in BMES2 and BMES3. Although a high content of pollutants can lead to the breeding of aerobic bacteria and the consumption of dissolved oxygen in water, if the pollutants are not in a form conducive to the absorption and utilization of aerobic bacteria, there may be less bacterial breeding, so as to maintain or increase the content of dissolved oxygen in the water. Therefore, it was necessary to further explore the chemical composition characteristics of the water quality.

No exogenous pollutants were added during the operation, and more than 90% of the test data showed that pH was stable between 7 and 8. The pH values in each reactor were similar, indicating that in this condition BMESs can achieve good control and stability of water pH.

EEM

EEM is used to analyze the composition type and content of dissolved organic matter based on fluorescence intensity information obtained from changes in excitation wavelength and emission wavelength. In this study, to explore the mechanism of water quality difference in each reactor, honeycomb-structure fluorescence spectrum scanning was performed(Fig. 5).

The fluorescence intensity of humic acid in Zone V of the BMES1 reactor was much higher than that of the other reactors. In the BMES2 reactor, there was an obvious humic acid fluorescence peak with a high fluorescence intensity (Ex. 260~265 nm/Em, 428~444 nm). Two obvious humic acid fluorescence peaks with high fluorescence intensity were observed for BMES3 (Ex. 260~270 nm/Em, 420~452 nm; Ex. 315~335 nm/Em, 408~430 nm). A distinct humic acid fluorescence peak with high fluorescence intensity was observed in BMES4 (Ex. 255~345 nm/Em, 400~470 nm). There was no obvious humic acid

fluorescence peak with high fluorescence intensity in BMES5, suggesting that the content of humic acid substances in the water in the reactor was relatively low. In BMES6, there were two obvious humic acid fluorescence peaks with high fluorescence intensity (Ex. 260~270 nm/Em, 422~448 nm; Ex. 315~330 nm/Em, 408~428 nm).

The EEM results show that the humus content changed in the order of BMES5 ▯ BMES2 ▯ BMES6 ▯ BMES3 ▯ BMES4 ▯ BMES1. The humus content of BMES1 was much higher than that of other reactors, and the content of EC and TOC in BMES1 was also higher than that of other reactors. At the same time, the water quality in BMES1 was the worst, indicating that a small anode area is not conducive to the removal of pollutants such as TOC and humus. On the other hand, the content of humus in BMES5 was the lowest, indicating that the honeycomb structure of the anode was conducive to controlling the release of humus and other pollutants in the sediments to the upper water body, reducing the content of humus in the water body. Different anode burial depths lead to different detection results of humic acid content. By comparing the EEM results of BMES4 and BMES3, BMES6, and BMES5, we found that a small anode burial depth (≤15 cm) is not conducive to the improvement of water quality and the removal of pollutants. At a burial depth of 7.5cm, the removal and control of humic acid in the reactor with a honeycomb-structure anode structure was better than that the reactor with a planar anode structure (humic acid content: BMES3 > BMES5). For a burial depth of 15 cm, the removal and control of humic acid in the reactor with honeycomb-structure anode structure was better than that in the reactor with the planar anode structure (humic acid content BMES4 > BMES6). In summary, a honeycomb-structure anode structure is more conducive to reducing and controlling humic acid substances in the upper water body of a BMES.

3.3 Sediment treatment

The anode is placed in the sediment at the bottom of a reactor so that it can be directly involved in the removal of contaminants from the sediment. In this study, the change in sediment pollutant content and water quality of the upper water body were monitored. Distilled water was used in the upper water body, and so it can be considered that the pollutants in the reactor water mainly came from the release of pollutants from the sediment. Changes in pollutant concentrations (TOC and TN) in the sediments during operation (40 days) and after operation (60 days) were monitored(Fig. 6).

The concentration of TOC was measured to indicate the total organic pollution in the sediment, which had background value of 3.37g /kg of dry sediment. Similar to the water layer, pollution in the sediment phase decreased during the operation. After 40 days of operation, removal rates of TOC in the sediments of BMES1 to BMES6 were 29.2%, 28.2%, 27.4%, 24.6%, 48.5%, and 30.4% (Table 3-2). After 60 days of operation, TOC removal rates of the sediments in each reactor were 24.3%, 23.0%, 23.0%, 23.7%, 53.1%, and 24.8%.

For reactors with a planar anode structure, anode depth had no obvious effect on TOC removal efficiency. However, for the honeycomb structure anode, a burial depth at 15 cm (BMES5) resulted in a sediment

TOC removal efficiency that was 2.1 times larger than that of an anode buried at 7.5 cm (BMES6). On this basis, the burial depths of anodes with a honeycomb structure should be no less than 15 cm.

In general, the removal efficiency of TOC from sediments in the BMES5 reactor was 20%~30% higher than that of the other reactors, confirming that this is a relatively efficient degradation method for TOC in sediments. Except for the BMES5 reactor, the other reactors all showed a slight increase of pollutants in the sediment during 60 days of operation compared with 40 days of operation. This may be attributed to the rapid removal of easily degraded pollutants in BMES within a short period of time, but with increased running time, the accumulation of refractory pollutants leads to a slight increase in the TOC content(Amy T. Kan. et al (1994). The honeycomb structure of the anode in the BMES5 reactor enabled greater contact with the sediments, which was beneficial for the pollutant removal efficiency. Furthermore, the advantage of the BMES5 reactor for TOC content control was highlighted, indicating that the continuous TOC effect in sediments is best when a honeycomb-structure anode is applied at a certain depth (15 cm).

The TN values in BMES systems constructed with different anode configurations were monitored. The TN content in the initial sediment was 2.3±0 g/kg. After 40 days of operation, the TN removal of sediments in BMES1 was not obvious, while TN removal rates in BMES2–BMES6 were 28.3%, 14.1%, 7.6%, 40.2%, and 14.1%. After 60 days of operation, the TN removal rates of sediments in BMES1–BMES6 were 26.1%, 20.7%, 26.1%, 24.8%, 46.7%, and 23.9%.

The removal efficiency of TN from the sediments of BMES5 on day 40 was 2.9 times that of BMES3; and the removal efficiency of TN from BMES5 on day 60 was 1.8 times that of BMES3. These results show that reactors constructed with a honeycomb-structure anode structure are more conducive to TN control in sediments.

Changes in the TN contents of sediments at different anode burial depths were also compared. For BMES3 and BMES4 (planar anode reactors), there was no significant difference in the removal effect of TN from sediments as a function of burial depth. From BMES5 and BMES6 (honeycomb-structure anode reactors), the removal efficiency of TN from sediments for an anode burial depth of 15 cm was twice as high as that for a burial depth of 7.5 cm. As such, we recommend that the burial depth of anodes with honeycomb structure should be more than 15 cm.

The removal efficiency of TN from sediments in the BMES5 reactor was 20%~33% higher than that of the other reactors. By comparing the removal efficiencies at 40 and 60 days, we found that the removal efficiency of TN in BMES5 increased by only 6.5% after 20 days of operation, while the removal efficiency of sediments in BMES1, BMES3, BMES4, and BMES6 increased by 30.1%, 12%, 14.2%, and 9.8%, respectively. Compared with other anode structures, the BMES5 reactor not only had a higher removal rate for TN removal in sediments, but also shortened the operating cycle. Thus, a honeycomb structure anode accelerates TN removal from sediments in BMES systems.

4 Conclusion

During the study, carbon mesh anodes with honeycomb-structure supports were compared with horizontal anodes, and the BMES was tested using different cover depths and anode densities.

During this study, it was found that the main reason affecting the performance of the reactor was the difference in the performance of the anode, and the performance of the anode with honeycomb-structure was the best. Three-dimensional anode can prevent pollutants from being released from sediments to the upper water body. Meanwhile, it is found that the removal efficiency of TOC and TN from sediments is 20%□30% higher in the reactor constructed by honeycomb-structure anode than that of other reactors. When the anode area of the planar structure was less than 50% of the remediation site (bottom area), it was not conducive to the electrochemical performance and pollutant removal performance of the system. However, the performance of BMES system is not maintained when the anode buried depth is 7.5cm, and the system performance is better when the anode buried depth is 15 cm.

Declarations

Acknowledgements

This work was supported by the Supported by Heilongjiang Touyan Team. The research was also supported by National Key Research and Development Program of China (Grant No. 2017ZX07403001). The authors also acknowledged the support of the Independent project of North China Municipal Engineering Design and Research Institute Co., LTD (HJ-2021-32-HJY) and Ministry of Housing and Urban-Rural Development research and development projects(2020-K-038).

References

1. Amy T, Kan G, Fu, Mason B Tomson(1994)Adsorption/Desorption Hysteresis in Organic Pollutant and Soil/Sediment.Environmental science and technology28:859–867
2. An J, Kim B, Nam J, Ng HY, Chang IS (2013) Comparison in performance of sediment microbial fuel cells according to depth of embedded anode. Bioresour Technol 127:138–142. doi:10.1016/j.biortech.2012.09.095
3. Beg MU, Al-Muzaini S, Saeed T, Jacob PG, Beg KR, Al-Bahloul M, Al-Matrouk K, Al-Obaid T, Kurian A (2001) Chemical contamination and toxicity of sediment from a coastal area receiving industrial effluents in Kuwait. Arch Environ Contam Toxicol 41(3):289–297. doi:10.1007/s002440010251
4. Bolam SG, Rees HL, Somerfield P, Smith R, Clarke KR, Warwick RM, Atkins M, Garnacho E (2006) Ecological consequences of dredged material disposal in the marine environment: a holistic assessment of activities around the England and Wales coastline. Mar Pollut Bull 52(4):415–426. doi:10.1016/j.marpolbul.2005.09.028
5. De Schamphelaire L, Rabaey K, Boeckx P, Boon N, Verstraete W (2008) Outlook for benefits of sediment microbial fuel cells with two bio-electrodes. Microb Biotechnol 1(6):446–462. doi:10.1111/j.1751-7915.2008.00042.x

6. Deng H, Wu Y-C, Zhang F, Huang Z-C, Chen Z, Xu H-J, Zhao F (2014) Factors Affecting the Performance of Single-Chamber Soil Microbial Fuel Cells for Power Generation. Pedosphere 24(3):330–338. doi:10.1016/s1002-0160(14)60019-9
7. Dong H, Yu H, Wang X, Zhou Q, Feng J (2012) A novel structure of scalable air-cathode without Nafion and Pt by rolling activated carbon and PTFE as catalyst layer in microbial fuel cells. Water Res 46(17):5777–5787. doi:10.1016/j.watres.2012.08.005
8. Feng C, Lv Z, Yang X, Wei C (2014) Anode modification with capacitive materials for a microbial fuel cell: an increase in transient power or stationary power. Phys Chem Chem Phys 16(22):10464–10472. doi:10.1039/c4cp00923a
9. Holmes DE, Bond DR, Lovley DR (2004) Electron Transfer by Desulfobulbus propionicus to Fe(III) and Graphite Electrodes. Appl Environ Microbiol 70(2):1234–1237. doi:10.1128/aem.70.2.1234-1237.2004
10. Hutchinson AJ, Tokash JC, Logan BE (2011) Analysis of carbon fiber brush loading in anodes on startup and performance of microbial fuel cells. J Power Sources 196(22):9213–9219. doi:10.1016/j.jpowsour.2011.07.040
11. Karthikeyan R, Wang B, Xuan J, Wong JWC, Lee PKH, Leung MKH (2015) Interfacial electron transfer and bioelectrocatalysis of carbonized plant material as effective anode of microbial fuel cell. Electrochim Acta 157:314–323. doi:10.1016/j.electacta.2015.01.029
12. Kouzuma A, Kaku N, Watanabe K (2014) Microbial electricity generation in rice paddy fields: recent advances and perspectives in rhizosphere microbial fuel cells. Appl Microbiol Biotechnol 98(23):9521–9526. doi:10.1007/s00253-014-6138-0
13. Leang C, Adams LA, Chin KJ, Nevin KP, Methe BA, Webster J, Sharma ML, Lovley DR (2005) Adaptation to disruption of the electron transfer pathway for Fe(III) reduction in Geobacter sulfurreducens. J Bacteriol 187(17):5918–5926. doi:10.1128/JB.187.17.5918-5926.2005
14. Li WW, Yu HQ (2015) Stimulating sediment bioremediation with benthic microbial fuel cells. Biotechnol Adv 33(1):1–12. doi:10.1016/j.biotechadv.2014.12.011
15. Lovley DR (2006) Bug juice: harvesting electricity with microorganisms. Nat Rev Microbiol 4(7):497–508. doi:10.1038/nrmicro1442
16. Martins G, Peixoto L, Brito AG, Nogueira R (2014a) Phosphorus–iron interaction in sediments: can an electrode minimize phosphorus release from sediments? Reviews in Environmental Science and Bio/Technology 13(3):265–275. doi:10.1007/s11157-014-9343-5
17. Martins G, Peixoto L, Teodorescu S, Parpot P, Nogueira R, Brito AG (2014b) Impact of an external electron acceptor on phosphorus mobility between water and sediments. Bioresour Technol 151:419–423. doi:10.1016/j.biortech.2013.10.048
18. Oon YL, Ong SA, Ho LN, Wong YS, Dahalan FA, Oon YS, Lehl HK, Thung WE (2016) Synergistic effect of up-flow constructed wetland and microbial fuel cell for simultaneous wastewater treatment and energy recovery. Bioresour Technol 203:190–197. doi:10.1016/j.biortech.2015.12.011

19. Sajana TK, Ghangrekar MM, Mitra A (2014) Effect of presence of cellulose in the freshwater sediment on the performance of sediment microbial fuel cell. Bioresour Technol 155:84–90. doi:10.1016/j.biortech.2013.12.094
20. Song T-s, Tan W-m, Wu X-y, Zhou CC (2012) Effect of graphite felt and activated carbon fiber felt on performance of freshwater sediment microbial fuel cell. Journal of Chemical Technology & Biotechnology 87(10):1436–1440. doi:10.1002/jctb.3764
21. Song TS, Yan ZS, Zhao ZW, Jiang HL (2011) Construction and operation of freshwater sediment microbial fuel cell for electricity generation. Bioprocess Biosyst Eng 34(5):621–627. doi:10.1007/s00449-010-0511-x
22. Rice EW, Baird RB, Eaton AD (2017) Standard Methods for the Examination of Water and Wastewater. American Water Works Association, Water Environment Federation, American Public Health Association
23. Teleken JT, Silva JdS, Fraga MF, Ogrodowski CS, Santana FB, Carciofi BAM (2017) Mathematical Modeling Of the Electric Current Generation In a Microbial Fuel Cell Inoculated with Marine Sediment. Braz J Chem Eng 34(1):211–225. doi:10.1590/0104-6632.20170341s20150377
24. Bingchuan L n, Isaiah Williams b, Yan Li b, Lei Wang c, Amvrossios Bagtzoglou b(2016)Towards high power output of scaled-up benthic microbial fuel cells (BMFCs) using multiple electron collectors.Biosensors and Bioelectronics79:439–441. doi: 10.1016/j.bios.2015.12.077
25. Villasenor J, Capilla P, Rodrigo MA, Canizares P, Fernandez FJ (2013) Operation of a horizontal subsurface flow constructed wetland–microbial fuel cell treating wastewater under different organic loading rates. Water Res 47(17):6731–6738. doi:10.1016/j.watres.2013.09.005
26. Virdis B, Rabaey K, Yuan Z, Keller J (2008) Microbial fuel cells for simultaneous carbon and nitrogen removal. Water Res 42(12):3013–3024. doi:10.1016/j.watres.2008.03.017
27. Yang Y, Lu Z, Lin X, Xia C, Sun G, Lian Y, Xu M (2015) Enhancing the bioremediation by harvesting electricity from the heavily contaminated sediments. Bioresour Technol 179:615–618. doi:10.1016/j.biortech.2014.12.034
28. Zabihallahpoor A, Rahimnejad M, Talebnia F (2015) Sediment microbial fuel cells as a new source of renewable and sustainable energy: present status and future prospects. RSC Adv 5(114):94171–94183. doi:10.1039/c5ra15279h
29. Zhang Y, Wang X, Li X, Cheng L, Wan L, Zhou Q (2015) Horizontal arrangement of anodes of microbial fuel cells enhances remediation of petroleum hydrocarbon-contaminated soil. Environ Sci Pollut Res Int 22(3):2335–2341. doi:10.1007/s11356-014-3539-7
30. Zhu D, Wang DB, Song TS, Guo T, Ouyang P, Wei P, Xie J (2015) Effect of carbon nanotube modified cathode by electrophoretic deposition method on the performance of sediment microbial fuel cells. Biotechnol Lett 37(1):101–107. doi:10.1007/s10529-014-1671-6

Figures

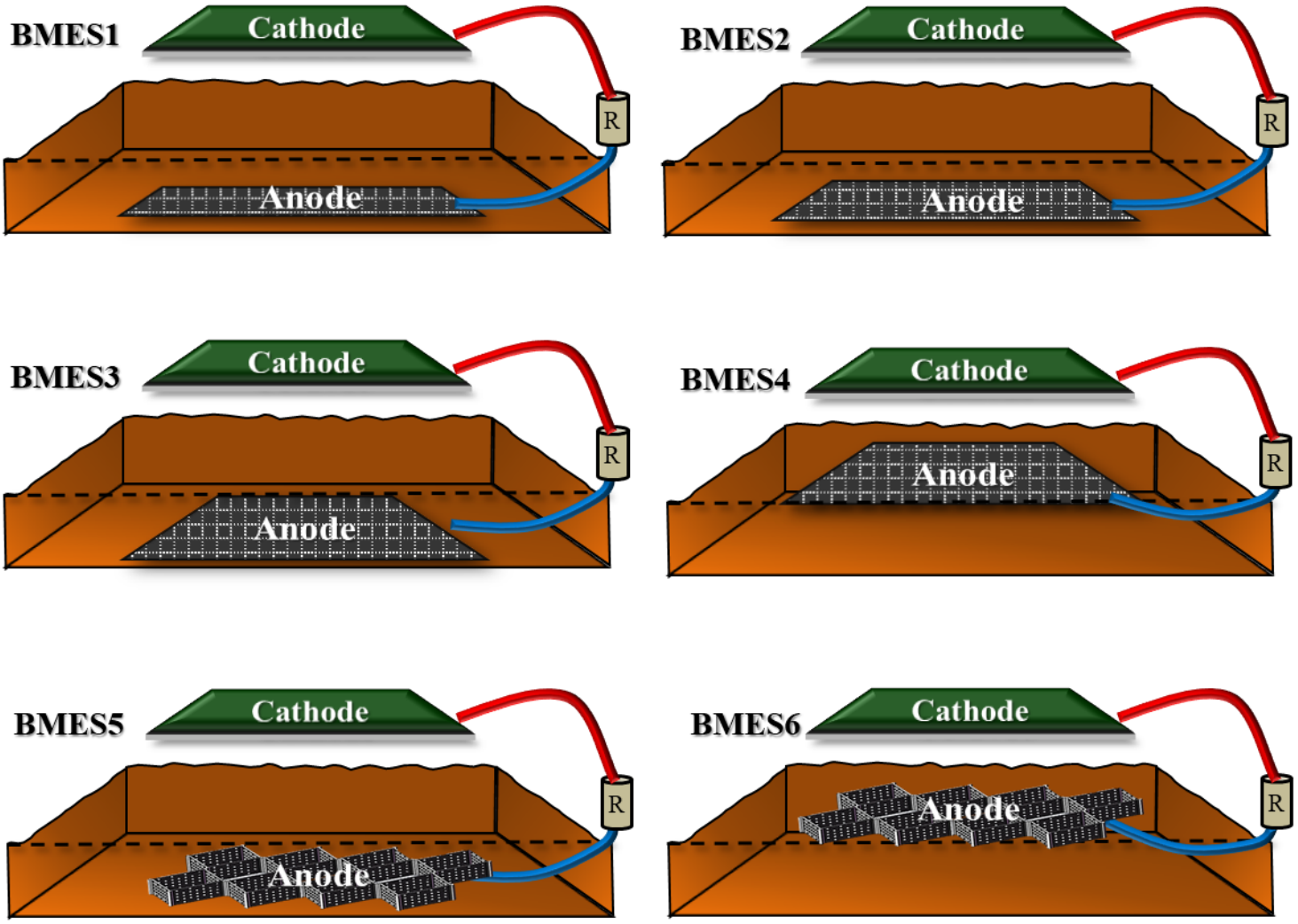

Figure 1

The dimension of the schematic of pilot-scale BMES.

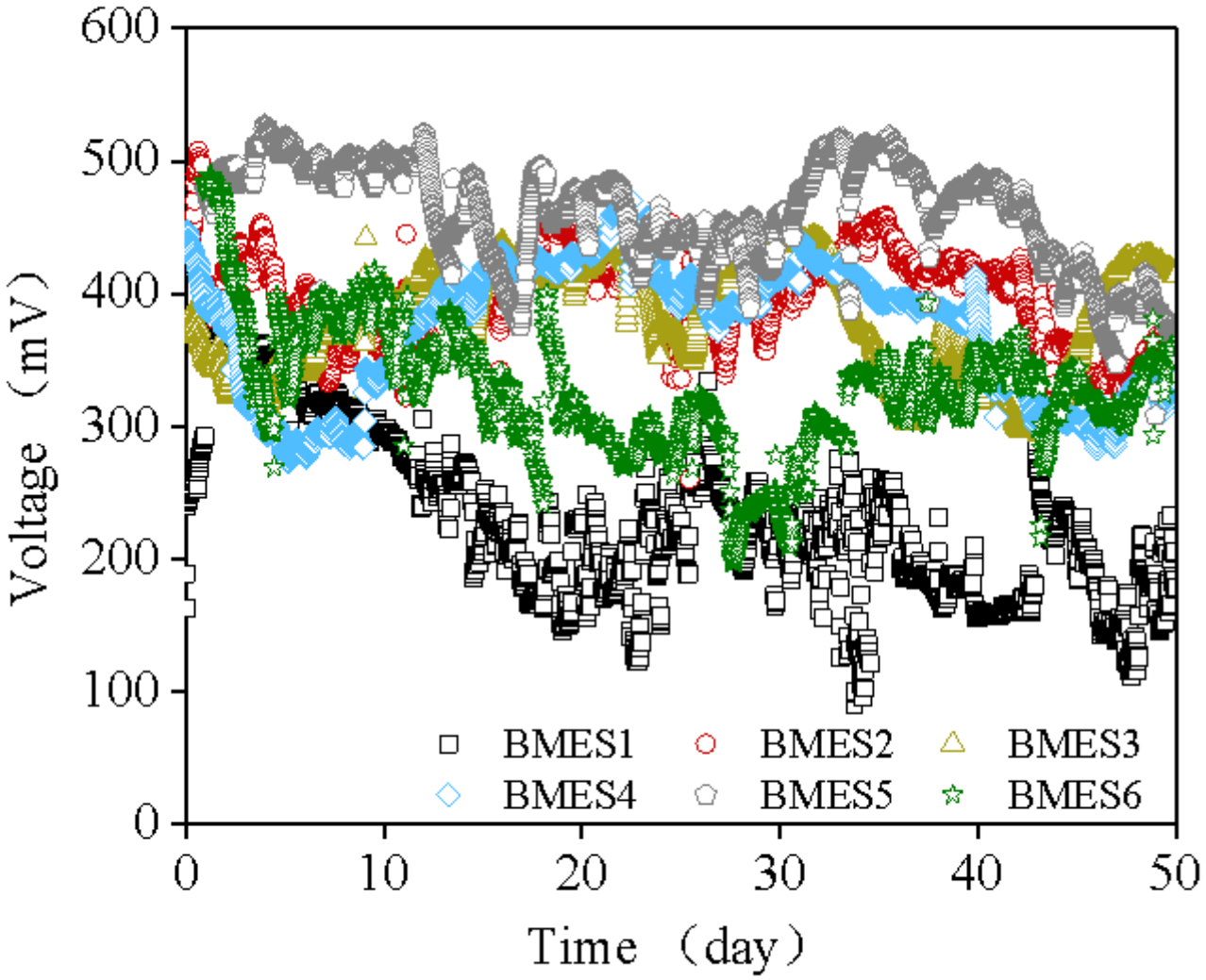

Figure 2

Voltage change during the operation.

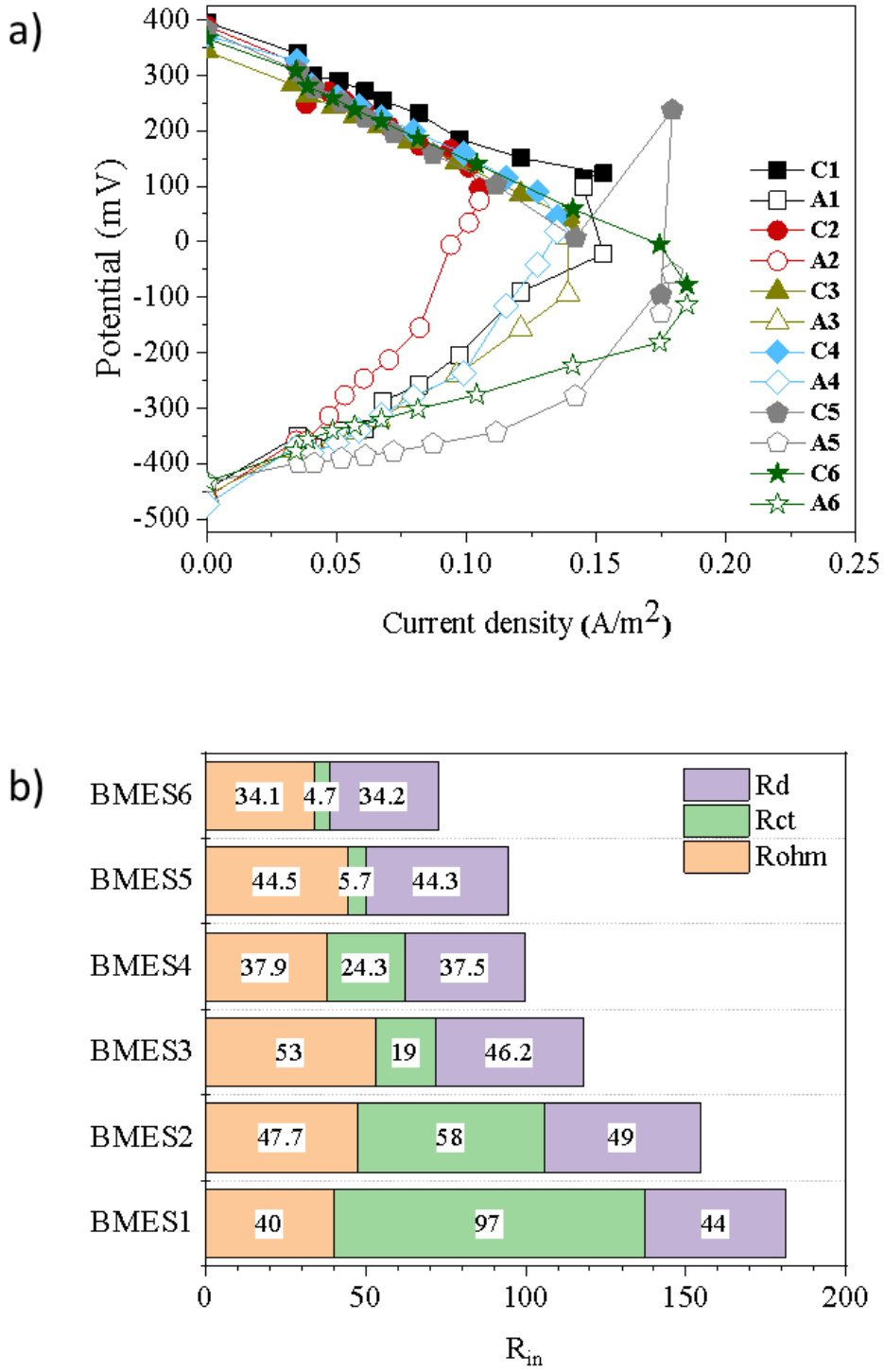

Figure 3

Electrochemical performance of the BMESs. a) EIS of anode in different reactors; b) Rd、Rct and Rohm in different reactors..

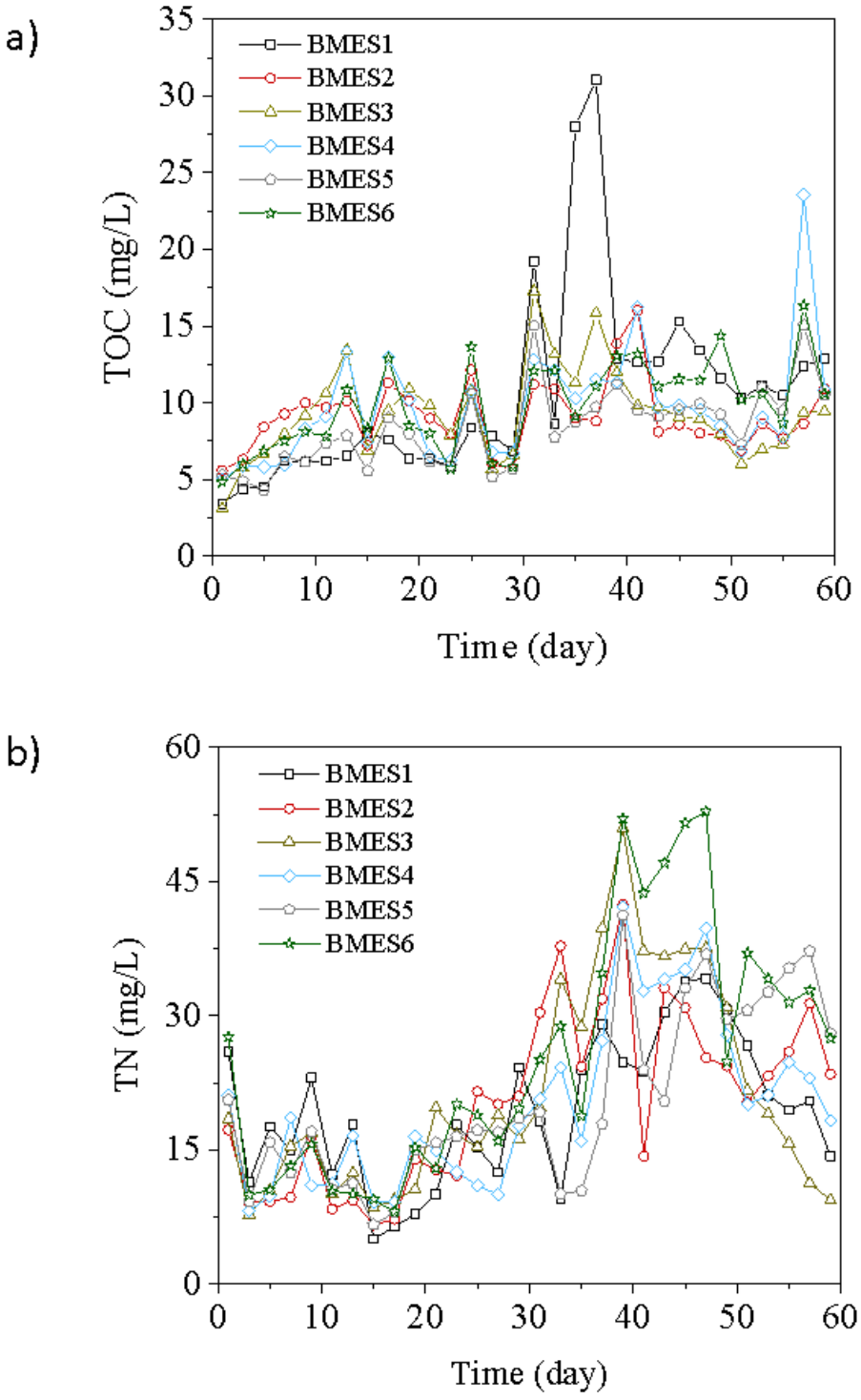

Figure 4

TOC and TN change in water during the operation.

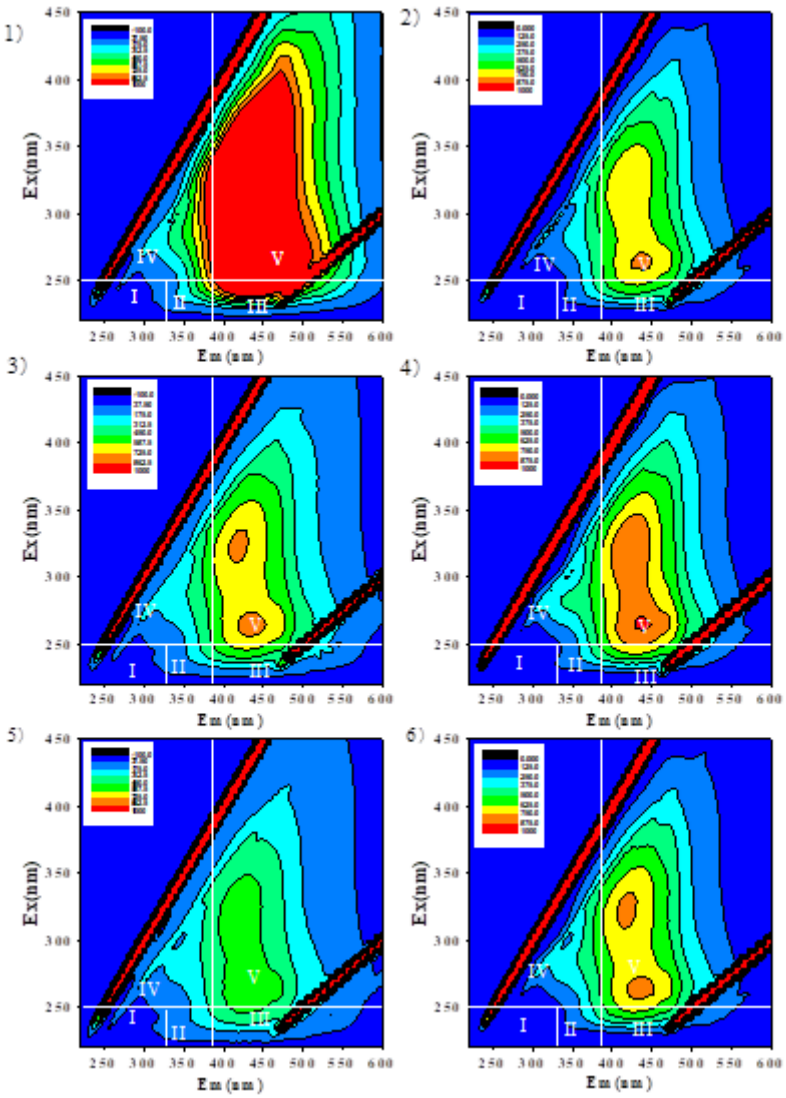

Figure 5

EEM contour during operation. (1)BMES1□(2)BMES2□(3)BMES3□(4)BMES4□(5)BMES5□(6)BMES6.

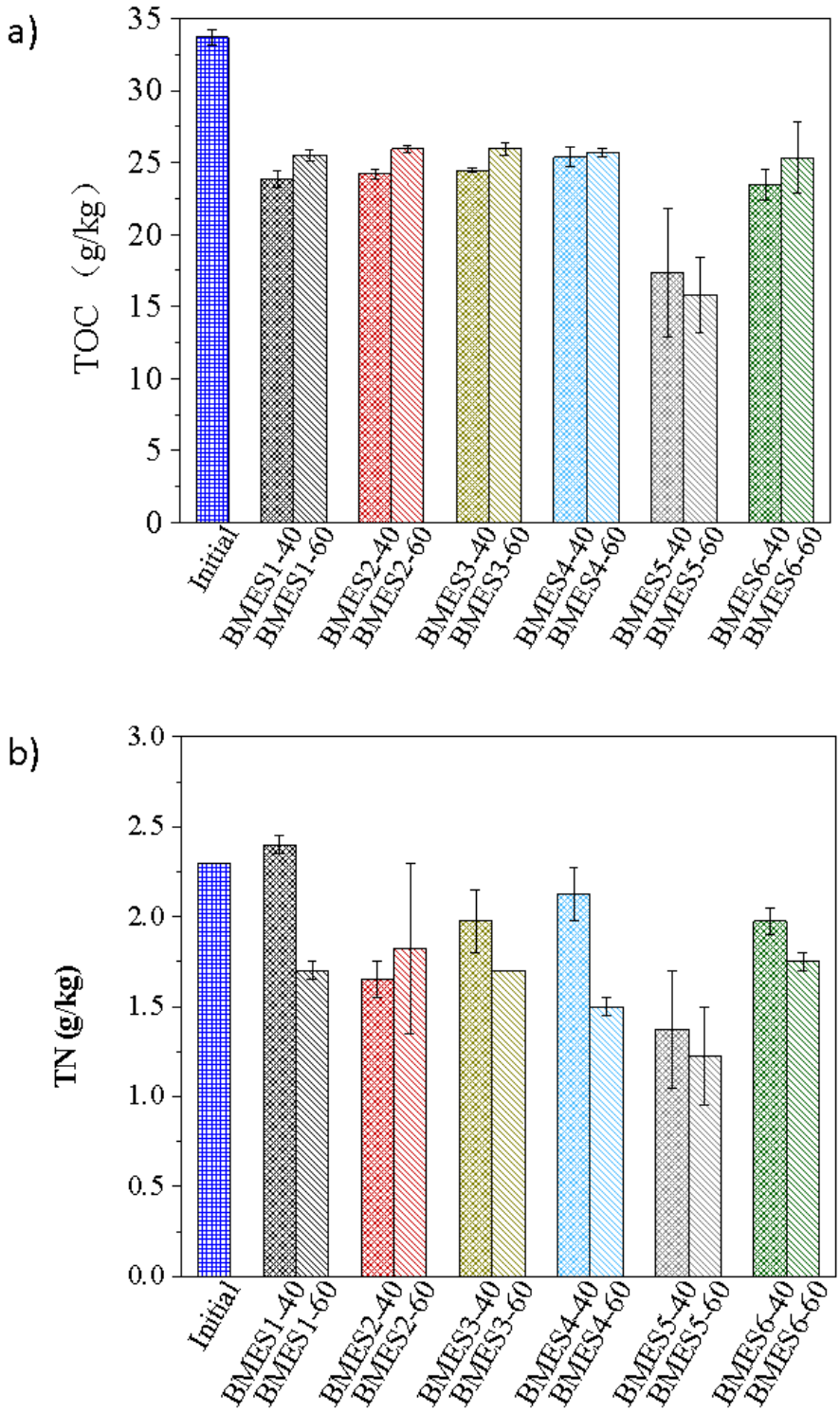

Figure 6

TOC and TN concentration changes in sediments. a) TOC concentration changes in sediments; b) TN concentration changes in sediments

Supplementary Files

This is a list of supplementary files associated with this preprint. Click to download.

- Supportmaterial.docx